Macromolecules

Article

pubs.acs.org/Macromolecules

An Acetylene-Containing Perylene Diimide Copolymer for High Mobility n-Channel Transistor in Air

Xingang Zhao,[†,§] Lanchao Ma,[†,§] Lei Zhang,[†,§] Yugeng Wen,[†,§] Jianming Chen,[†,§] Zhigang Shuai,[⊥] Yunqi Liu,*[,†] and Xiaowei Zhan*[,†,‡]

[†]Beijing National Laboratory for Molecular Sciences and CAS Key Laboratory of Organic Solids, Institute of Chemistry, Chinese Academy of Sciences, Beijing 100190, China

[§]University of Chinese Academy of Sciences, Beijing 100049, China

[⊥]Department of Chemistry, Tsinghua University, Beijing 100084, China

[‡]Department of Materials Science and Engineering, College of Engineering, Peking University, Beijing 100871, China

Supporting Information

ABSTRACT: A new solution-processable conjugated copolymer (**P1**) of perylene diimide (PDI) and dithienothiophene (DTT) incorporating acetylene spacers was synthesized by palladium(0)-catalyzed Sonogashira coupling reaction. Theory calculation reveals that introduction of rod-like ethynylene spacer in the polymer main chain promotes planarity and π-conjugation of the polymer main chain. Relative to the conjugated copolymer (**P2**) of PDI and DTT without acetylene spacers, polymer **P1** exhibits 0.1 eV down shift of LUMO level and 89 nm red shift of low-energy absorption band. Polymer **P1** in top-contact bottom-gate organic field-effect transistors (OFETs) exhibits a saturation electron mobility of 0.06 $cm^2\ V^{-1}\ s^{-1}$ in air, while **P2** does not function in the same device in air. Additionally, a saturation electron mobility of 0.075 $cm^2\ V^{-1}\ s^{-1}$ in air, and after six days storage in air, an electron mobility of 0.034 $cm^2\ V^{-1}\ s^{-1}$ were observed for **P1** in bottom-contact bottom-gate OFETs; while a saturation electron mobility of 0.038 $cm^2\ V^{-1}\ s^{-1}$ in air, and after six days storage in air, an electron mobility of 0.013 $cm^2\ V^{-1}\ s^{-1}$ were observed for **P2** in the same device. The better air stability and higher electron mobility of **P1** are attributed to densely ordered packing of the polymer chains excluding oxygen or water and the lower LUMO level of **P1**.

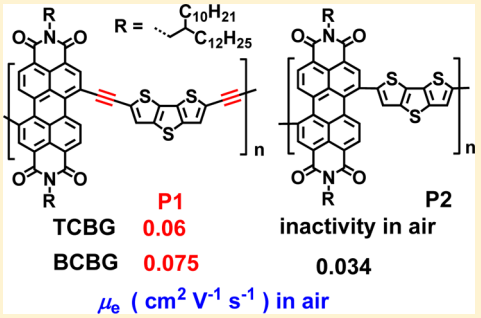

INTRODUCTION

Compared with traditional inorganic materials based microelectronics, optoelectronic devices based on conjugated polymers are a promising candidate which has advantages of low cost, lightweight, solution processability and flexibility.[1−4] Conjugated polymers can be classified as hole (p-type) or electron (n-type) transporting materials according to the type of orderly migrating charge carriers under a given set of conditions. Hole transporting conjugated polymer semiconductors have seen a revolutionary rise in performance over the past two decades; some p-type polymers show extremely high hole mobility (>1 $cm^2\ V^{-1}\ s^{-1}$),[5−8] approximate to that of amorphous silicon. However, the electron mobilities of n-type semiconducting polymers have lagged behind those of their p-type counterparts. In particular, air stable, high-mobility n-type polymer semiconductors remain very rare.[9−14] Considering the importance of n-type organic materials in the fabrication of organic p−n junctions, solar cells, n-channel organic field-effect transistors (OFET) and complementary logic circuits, the development of high-performance electron-transport semiconductors is one of the biggest challenges in organic electronics.[15−17]

Rylene diimides combine highly planar π-conjugated cores (naphthalene, perylene etc.) with electron-withdrawing tetracarboxydiimide; substituents on imide nitrogen can manipulate solubility, morphology, and solid-state packing without disrupting backbone electronic conjugation.[18] Rylene diimides are a robust, versatile class of n-type materials with excellent stability, low LUMOs and, in some cases, high electron mobilities; they are, therefore, promising candidates for a variety of organic electronics applications.[18−20] Several n-type conjugated polymers based on perylene diimides (PDIs)[9,21−23] and naphthalene diimides (NDIs)[11,24−27] have been synthesized and used in n-channel OFETs. For example, Zhan et al. reported the synthesis of the first soluble rylene diimide-based fully conjugated copolymer; this PDI-dithienothiophene (DTT) copolymer (**P2**, Chart 1) in bottom-gate top-contact OFETs exhibited a saturation electron mobility of 0.013 $cm^2\ V^{-1}\ s^{-1}$ and a low threshold voltage of 4 V in nitrogen.[21] Later, Facchetti and co-workers reported a copolymer of NDI and bithiophene; OFETs in top-gate bottom-contact on polymeric

Received: November 24, 2012
Revised: March 1, 2013
Published: March 8, 2013

Chart 1. Chemical Structure of P1 and P2

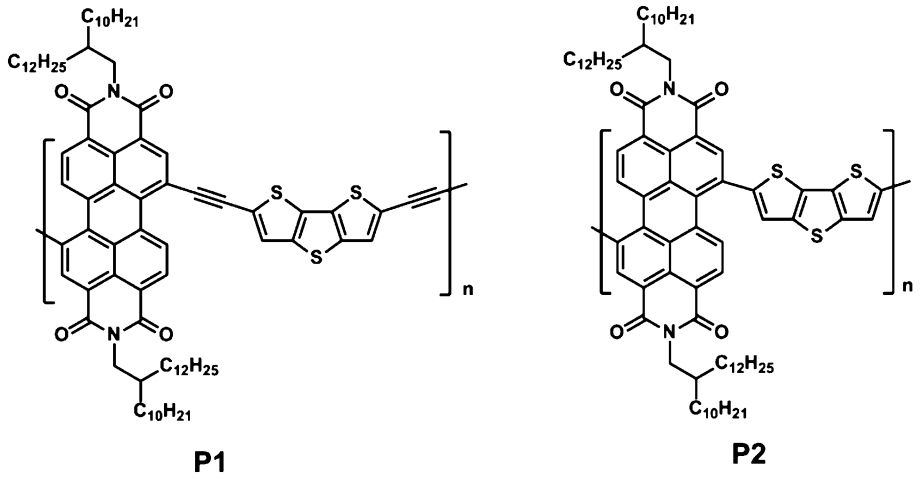

Scheme 1. Synthesis of P1

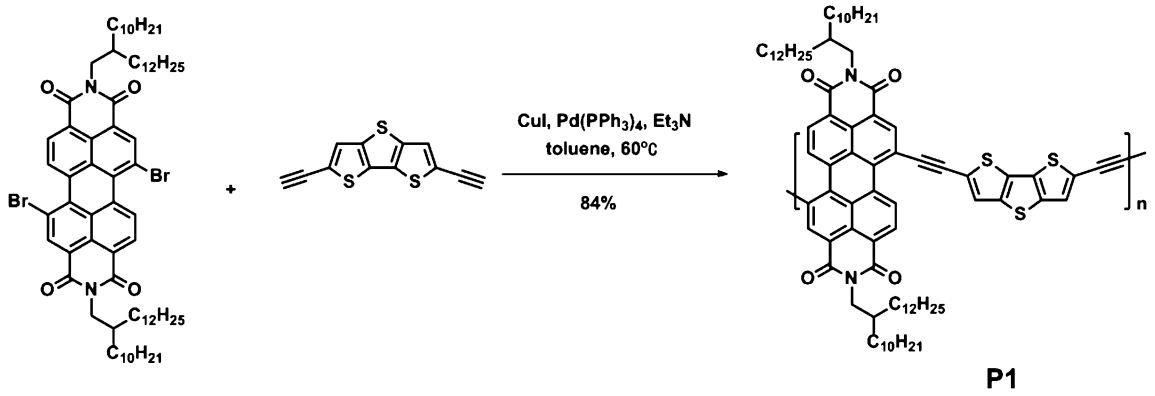

dielectrics device configuration exhibited electron mobilities of 0.10−0.85 $cm^2\ V^{-1}\ s^{-1}$ under ambient conditions with on/off ratios $>10^6$.[11]

Poly(arylene ethynylene)s with triple bonds in main chains have attracted increasing interest during the past few decades as a promising class of semiconductors. The incorporation of ethynylene π-spacers offers a viable approach to induce planarity, enhance π-conjugation along the polymer chain and thus charge carrier mobility.[28,29] Furthermore, LUMO levels may be lowered by the presence of electron-withdrawing triple bond spacers.[30,31] Recently, a paucity of PDI or NDI oligomers and copolymers incorporating ethynylene spacers has been reported.[30−34] These semiconductors exhibited the highest electron mobility of 0.1 ± 0.05 $cm^2\ V^{-1}\ s^{-1}$ in nanowire OFETs.[35]

Here, we report a new soluble n-type PDI copolymer (**P1**, Chart 1) by introducing ethynylene spacers between the electron acceptor PDI units and the electron donor DTT units in **P2** in order to reduce the steric hindrance between PDI and DTT units, promote planarity and enhance the π-conjugation along the polymer main chain. Relative to **P2**, **P1** exhibits lower LUMO level, higher electron mobility and better ambient stability. Bottom-gate top-contact OFETs based on **P1** exhibits a saturation electron mobility of 0.06 $cm^2\ V^{-1}\ s^{-1}$ in air, while **P2** does not function in the same device in air. Bottom-gate bottom-contact OFETs based on **P1** exhibits a saturation electron mobility of 0.075 $cm^2\ V^{-1}\ s^{-1}$ in air, while **P2** exhibits a saturation electron mobility of 0.038 $cm^2\ V^{-1}\ s^{-1}$ in the same device in air. To the best of our knowledge, electron mobility of 0.075 $cm^2\ V^{-1}\ s^{-1}$ is among the highest reported for bottom-gate OFETs based on n-type conjugated polymers in air.

RESULTS AND DISCUSSION

Synthesis and Characterization. It is well-known that the PDI bromination procedure gives a mixture of 1,7 and 1,6 regioisomers.[19,36] The ratio of 1,7- to 1,6-regioisomer in our PDI dibromide is 84%: 16%, determined by ^{1}H NMR (600 MHz) spectroscopy. We did not separate 1,7- and 1,6-regioisomers and used their mixture for next polymerization since it is very hard to get isomer pure monomer. In view of 1,7-isomer is the major product, the isomer mixture was simplified as 1,7-isomer. The synthetic route for polymer **P1** is shown in Scheme 1. **P1** was synthesized in 84% yield through a Sonogashira coupling polymerization of *N*,*N*′-bis(2-decyltetradecyl)-1,7-dibromo-3,4:9,10-perylene diimide with 2,6-diethynyldithieno[3,2-*b*:2′,3′-*d*]thiophene in the presence of $Pd(PPh_3)_4$ catalyst. Polymer **P1** is soluble in common organic solvents such as chlorobenzene, chloroform, and THF and can readily be processed from solution. The number-average molecular weight (M_n), weight-average molecular weight (M_w), and polydispersity index (M_w/M_n) of **P1**, measured by gel permeation chromatography versus polystyrene standards, were 15 000, 17 000, and 1.1, respectively, similar to those of **P2**. Since we purified polymer **P1** and only collected the first part by size exclusion column chromatography, the molecular weight distribution is pretty narrow. The thermal stability of **P1**

dx.doi.org/10.1021/ma302428x | Macromolecules 2013, 46, 2152−2158

was determined using thermogravimetric analysis (Figure S1, Supporting Information); the decomposition temperature, defined as that at which initial 5% of weight loss, is higher than 300 °C under nitrogen. Differential scanning calorimetry (DSC) traces (Figure S2, Supporting Information) of **P1** show no evidence for any phase transitions or other processes up to 250 °C.

Calculation. To explore the molecular architecture of the polymers, density functional theory (DFT) calculations at the B3LYP/6-31G(d,p) level[37,38] with the Gaussian 09 program package[39] were performed for oligomer models (PDI−ethynylene−DTT−ethynylene−PDI and PDI−DTT−PDI, with *N*-methyl groups replacing *N*-2-decyltetradecyl) of **P1** and **P2**. The dihedral angles between PDI and DTT (θ_1 and θ_2, Figure 1, Table 1) in **P2** are 56.81° and 52.85°, much larger

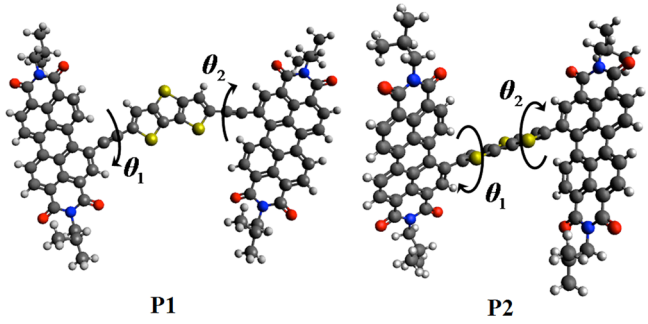

Figure 1. Optimized geometries at B3LYP/6-31G(d,p) level. The torsion parameters are labeled as θ_1 and θ_2.

Table 1. Frontier Orbitals and Torsion Profiles Obtained from DFT Calculations on P1 and P2 at B3LYP/6-31G(d,p) Level

	HOMO (eV)	LUMO (eV)	gap (eV)	θ_1 (deg)	θ_2 (deg)
P1	−5.57	−3.59	1.98	9.45	8.47
P2	−5.73	−3.53	2.20	56.81	52.85

than those (9.45° and 8.47°) in **P1**. Steric interaction between DTT and the bay-position neighboring hydrogen atom leads to a more twisted main chain in **P2.** The introduction of ethynylene spacer between PDI and DTT in **P1** reduces the steric hindrance between PDI and DTT units in **P2**, and induces coplanarity and rigidity of the main chain. The more planar conformation of the main chain leads to stronger interchain interaction in **P1** compared to **P2.** The calculated molecular orbital geometry and energy levels of the polymers is shown in Figure 2. The LUMO of **P1** is delocalized over the polymer backbones, while the LUMO of **P2** is located on the PDI units. Thus, **P1** exhibits lower LUMO, higher HOMO and smaller bandgap as a result of promoted planarity and enhanced π-conjugation along the polymer main chain relative to **P2**.

Absorption. The normalized UV−vis absorption spectra of **P1** and **P2** in dilute $CHCl_3$ solution and in thin film are illustrated in Figure 3. Introduction of ethynylene spacer between PDI and DTT in **P1** results in a considerable red shift of the low-energy maximum absorption in solution from 625 to 714 nm, stemmed from promoted planarity and enhanced π-conjugation along the polymer main chain. Additionally, the appearance of vibronic fine structure in the low-energy absorption band of **P1** in solution and film reveals greater backbone rigidity of **P1** induced by the rod-like ethynylene spacer relative to **P2.** The band at ca. 487 nm in **P2** with a

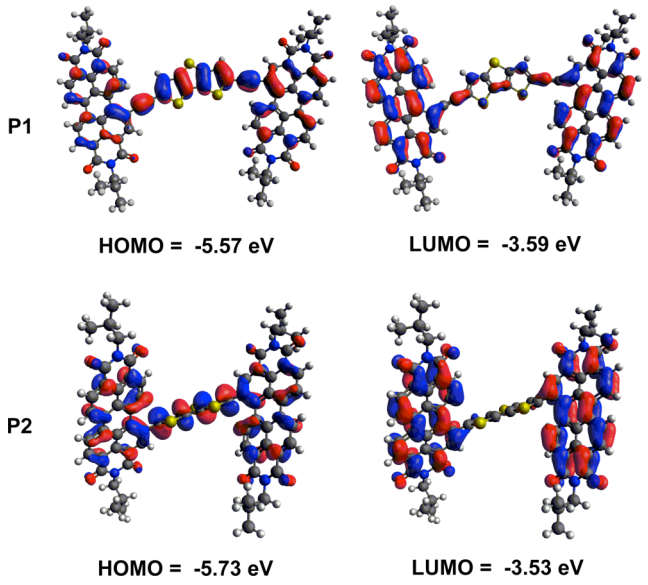

Figure 2. Molecular orbital geometry and energy levels obtained from DFT calculations on **P1** and **P2** at B3LYP/6-31G(d,p) level.

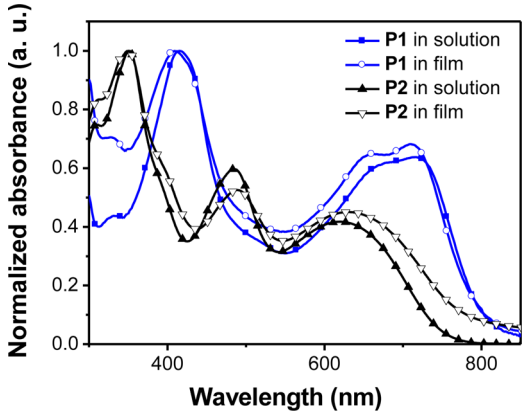

Figure 3. UV−vis absorption spectra of **P1** and **P2** in $CHCl_3$ solution and thin films.

twisted main chain in solution and film can be assigned to a principally PDI-based transition,[22] which is usually observed in D−A conjugated polymers based on PDI.[9,23,40,41] The disappearance of the peak at 487 nm in **P1** with a more planar main chain probably arises from the transition from electron localization to electron delocalization. A similar phenomenon was also observed in copolymers of PDI and bithiophene or terthiophene with or without ethynylene spacer.[32,42] The optical band gap estimated from the absorption onset edge of the thin film of **P1** is 1.55 eV, smaller than that (1.60 eV) of **P2**, indicating more extensive delocalization of the π-electrons in **P1**, which is in agreement with the calculation results.

Cyclic Voltammetry. The electrochemical property of **P1** was determined using cyclic voltammetry (CV) measurements in a film on a glassy-carbon working electrode. Polymer **P1** exhibited quasi-reversible reduction and irreversible oxidation waves (Figure 4), which is similar to **P2**,[21] revealing its potential as an electron transporting semiconductor. The onset oxidation and reduction potentials vs $FeCp_2^{+/0}$ are 1.0 and −0.8 V, respectively. Taking the absolute energy of the redox couple for $FeCp_2^{+/0}$ to be 4.8 eV below vacuum, the HOMO and LUMO were estimated to be −5.80 and −4.00 eV from the

dx.doi.org/10.1021/ma302428x | *Macromolecules* 2013, 46, 2152−2158

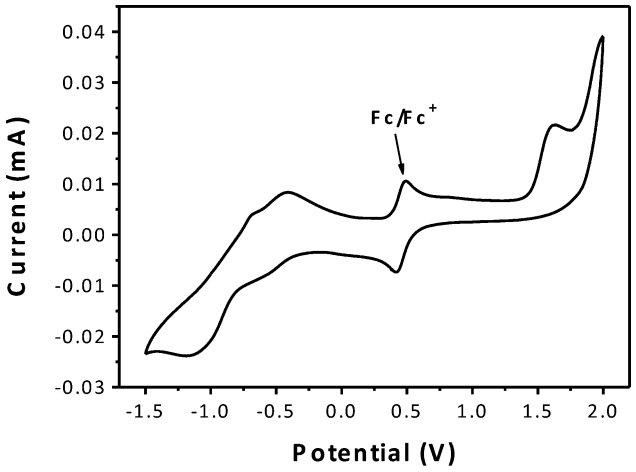

Figure 4. Cyclic voltammogram for **P1** in CH_3CN/0.1 M $[^nBu_4N]^+[PF_6]^-$ with ferrocenium/ferrocene as an internal standard, at 100 mV/s.

onset oxidation and reduction potentials, respectively. The HOMO is 0.10 eV higher but the LUMO is 0.10 eV lower than that of **P2** due to introduction of ethynylene units, showing the same trend as the computational prediction. The combination of deeper LUMO and more coplanarity of the polymer main chain caused by the presence of electron-withdrawing ethynylene units will be favorable to increase the ambient stability and electron mobility of **P1**.

Field-Effect Transistors. The electron mobilities of n-channel OFETs based on **P1** and **P2** were measured in top contact, bottom gate (TCBG) and bottom contact, bottom gate (BCBG) transistor configuration. OFET devices of **P1** and **P2** based on TCBG geometry were fabricated on octadecyltrichlorosilane (OTS)-modified SiO_2 (300 nm)/Si substrate by spin-coating a 10 mg/mL $CHCl_3$ solution. Gold (Au) was used as drain and source electrodes. The drain-source channel length (L) is 80 μm and width (W) is 8.8 mm. All the FET measurements were determined in ambient atmosphere (around 30% of humidity). Typical characteristic curves of **P1** in TCBG transistor are depicted in Figure 5. After annealing at 170 °C, an electron mobility of 0.06 $cm^2\ V^{-1}\ s^{-1}$, on/off current ratio of 10^5 and low threshold voltage of 4 V in the saturation regime were obtained. In contrast, polymer **P2** in TCBG OFETs exhibited an electron mobility of 0.017 $cm^2\ V^{-1}\ s^{-1}$, on/off current ratio of 10^6 and threshold voltage of 13 V in N_2 atmosphere, but showed complete inactivity in air. TCBG OFETs based on **P1** exhibit moderate air stability (Figure S3, Supporting Information). The electron mobilities of **P1** in TCBG OFETs have a sharp drop after 2 days storage in air, which is 9.2% of the initial value. However, there was almost no obvious variation in the following four days, and the on/off current ratio still kept at 10^5–10^6. Higher electron mobilities and enhanced air stability could be expected for isomer pure 1,7-linked **P1** due to a more π-conjugated structure and stronger assembly of a regioregular polymer backbone relative to the regioirregular (1,6- + 1,7-linked) **P1**.[43]

BCBG transistor configuration was also employed to measure the electron mobility of **P1** and **P2**. BCBG OFETs based on **P1** and **P2** were fabricated on OTS-treated SiO_2/Si substrates. The polymer activity layer was spin-coated from $CHCl_3$ solution (10 mg/mL). Gold/Ti was used as the source and drain electrodes. The channel length (L) was 38 μm; and

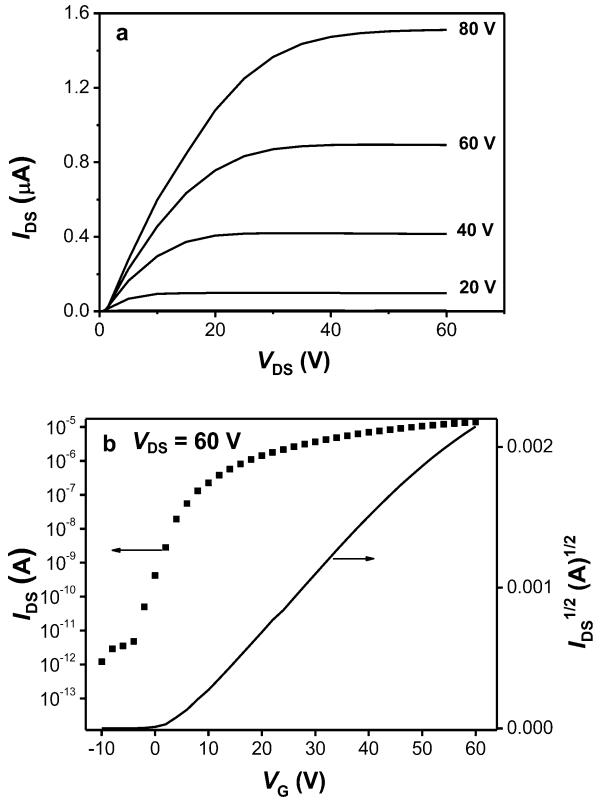

Figure 5. Typical current–voltage characteristics (I_{DS} vs V_{DS}) at different gate voltages (V_G), and I_{DS} and $(I_{DS})^{1/2}$ vs V_G plots at V_{DS} of 60 V for a top contact device based on **P1**.

the channel width (W) was 1400 μm. Typical characteristic curves of **P1** and **P2** in BCBG transistor are depicted in Figure S4 and S5 in Supporting Information. An electron mobility of 0.075 $cm^2\ V^{-1}\ s^{-1}$, on/off current ratio of 10^6 and threshold voltage of 14 V were achieved for **P1** in this device geometry in ambient atmosphere after annealing at 170 °C; the electron mobility is slightly higher than that of **P1** in TCBG configuration. In contrast, **P2** in BCBG OFETs exhibited an electron mobility of 0.038 $cm^2\ V^{-1}\ s^{-1}$, on/off current ratio of 10^6 and threshold voltage of 11 V in air after annealing at 170 °C. The mobility of 0.038 $cm^2\ V^{-1}\ s^{-1}$ for **P2** is only half of that for **P1** in the same device configuration.

BCBG OFETs based on **P1** and **P2** exhibited good air stability (Figure S6, Supporting Information). The electron mobilities of **P1** in BCBG OFETs have a sharp drop after one day storage in air, which is 68% of the initial value. However, there was almost no obvious variation in the following three days, and finally high electron mobility of 0.034 $cm^2\ V^{-1}\ s^{-1}$ and high on/off current ratio of ca. 10^6 were still observed after six days storage in ambient atmosphere. The evolution of the electron mobilities of **P2** over the time exposing to air showed the same trend as that **P1** exhibited. Surprisingly, after exposure to air for six days, a BCBG transistor based on **P2** still maintained a high electron mobility of 0.013 $cm^2\ V^{-1}\ s^{-1}$, which is ca. one-third of that for **P1** in the same condition. Obviously, BCBG OFETs based on **P1** and **P2** showed higher electron mobilities and better air stability than those with TCBG configuration. It is speculated that, for BCBG OFETs, the conducting channel (ca. a few nanometers) could be encapsulated by ca. 100 nm active organic semiconductor

dx.doi.org/10.1021/ma302428x | Macromolecules 2013, 46, 2152–2158

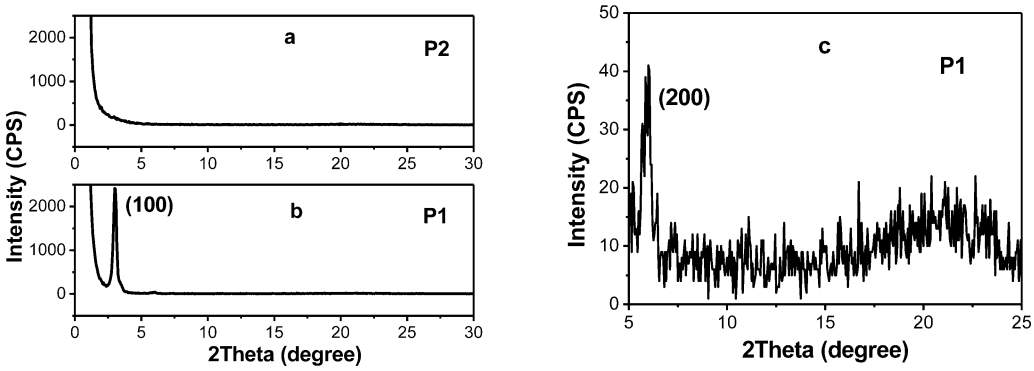

Figure 6. GIXRD patterns of **P1** and **P2** films annealed at 170 °C on OTS-modified Si/SiO_2 substrates.

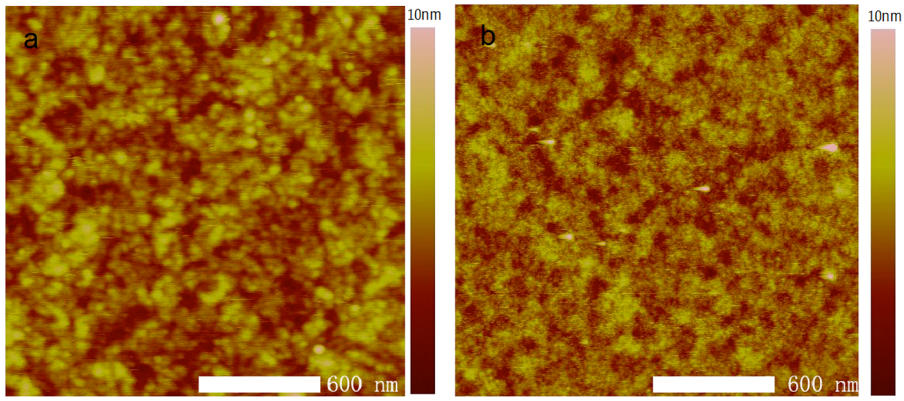

Figure 7. AFM topographic images of **P1** (a) and **P2** (b) films annealed at 170 °C on OTS-modified Si/SiO_2 substrates.

thin film spin-coated on the top of the devices against penetration of H_2O and O_2.

Film Morphology. Grazing incidence X-ray diffraction (GIXRD) (Figure 6) and atomic force microscopy (AFM) (Figure 7) of **P1** and **P2** films annealed at 170 °C were employed to characterize the microstructure and surface morphology of the active layer. In the out-of-plane scattering profile from the GIXRD, strong first diffraction peak (100) at $2\theta = 2.96°$ was observed for **P1** (Figure 6b), corresponding to a *d*-spacing (the lamellar repeating distance between the polymer chains) of 2.94 nm. The weak second diffraction peak (200) at $2\theta = 5.98°$ was also observed for **P1** (Figure 6c). Additionally, lacking of significant diffraction intensity in the in-plane scattering profiles suggests that **P1** had predominantly edge-on packing in film relative to the substrates.[44] However, no diffraction peaks were observed in the out-of-plane (Figure 6a) and in-plane scattering profiles of **P2**. Thus, polymer **P1** has ordered crystalline structure while **P2** has amorphous structure lacking of order. The stronger intermolecular interactions and more ordered packing are attributed to the coplanarity of the **P1** polymer main chain with rod-like ethynylene units.

As illustrated in the AFM images of annealed **P1** films, an entangled nodule-like morphology with a broad distribution of aggregate domains ranging from ca. 80 to 400 nm was observed, stemmed from the strong intermolecular interaction between the more planar **P1** polymer main chains. Compared to annealed **P2** films without obvious crystalline domains, the **P1** film showed more and larger interconnecting domains, which is consistent with the GIXRD results. The densely ordered packing can exclude oxygen or water in **P1** film and enhance mobilities and air stability.

CONCLUSION

A new solution-processable PDI copolymer incorporating acetylene spacers was synthesized. Introduction of rod-like ethynylene spacers in the polymer main chain reduces the steric hindrance between PDI and DTT units, promotes planarity and enhances the π-conjugation along the polymer main chain. As a result, the low-energy maximum absorption of **P1** in solution red shifts 89 nm and LUMO down shifted by 0.10 eV relative to those of **P2**. GIXRD and AFM reveal that annealed **P1** films exhibit an entangled nodule-like crystalline morphology with densely ordered packing, while annealed **P2** films exhibit an amorphous morphology lacking of order. Combination of low-lying LUMO energy level and the dense packing in the solid state could improve mobilites and air stability. As a result, **P1** in top-contact bottom-gate OFETs exhibited a saturation electron mobility of 0.06 $cm^2\ V^{-1}\ s^{-1}$ in air. In contrast to **P1**, **P2** did not function in the same devices in air although it exhibited electron mobilities of 0.017 $cm^2\ V^{-1}\ s^{-1}$ in nitrogen. Electron mobilities of 0.075 and 0.038 $cm^2\ V^{-1}\ s^{-1}$ were achieved in **P1** and **P2**-based bottom contact, bottom gate OFETs in ambient atmosphere, respectively. The electron mobilities of **P1** are among the highest reported for bottom-gate OFETs based on n-type conjugated polymers in air. BCBG OFETs based on **P1** and **P2** exhibited better air stability than TCBG devices. After 6 days storage in air, an electron mobility of 0.034 $cm^2\ V^{-1}\ s^{-1}$ and high on/off current ratio of ca. 10^6 were still observed for **P1** in BCBG OFETs, while an electron mobility of 0.013 $cm^2\ V^{-1}\ s^{-1}$ was observed for **P2** in the same device.

dx.doi.org/10.1021/ma302428x | *Macromolecules* 2013, 46, 2152−2158

EXPERIMENTAL SECTION

Materials. Unless stated otherwise, starting materials were obtained commercially and were used without further purification. Triethylamine was distilled from calcium hydride and toluene was distilled from sodium-benzophenone under nitrogen prior to use. 2,6-Diethynyldithieno[3,2-*b*:2′,3′-*d*]thiophene[45] and *N*,*N*′-bis(2-decyl-tetradecyl)-1,7-dibromo-3,4:9,10-perylene diimide[21] were synthesized according to our published procedures.

Characterization. The ^{1}H NMR spectra was recorded on a Bruker DMX 300 MHz or Bruker AVANCE 600 MHz spectrometer. Elemental analysis was carried out using a FLASH EA1112 elemental analyzer. Thermogravimetric analysis (TGA) measurements were performed on Shimadzu thermogravimetric analyzer (model DTG-60) under a nitrogen flow at a heating rate of 10 °C/min. Differential scanning calorimetry (DSC) measurements were performed using an METTLER differential scanning calorimeter (DSC822e) under a nitrogen atmosphere with a heating and cooling rate of 10 °C/min. Solution (chloroform) and thin-film (on quartz substrate) UV−vis absorption spectra were recorded on a JASCO V-570 spectrophotometer. Electrochemical measurements were carried out under nitrogen in a deoxygenated solution of tetra-*n*-butylammonium hexafluorophosphate (0.1 M) in acetonitrile using a computer-controlled CHI660C electrochemical workstation, a thin film of the sample coated on glassy-carbon working electrode, a platinum-wire auxiliary electrode, and an Ag wire anodized with AgCl as a pseudoreference electrode. The gel permeation chromatography (GPC) measurements were performed on a Waters 515 chromatograph connected to a Waters 2414 refractive index detector, using THF as eluent and polystyrene standards as calibrants; three Waters Styragel columns (HT2, 3, 4) connected in series were used. X-ray diffraction (XRD) measurements of thin films were performed in reflection mode using a D/MAX-TTR III Rigaku X-ray diffractometer. Grazing incidence X-ray diffraction pattern of organic thin films were obtained at a constant incidence angle of 0.2° ($\lambda = 2d[\sin\theta] = 1.54$ Å). AFM images of organic thin films were obtained on a NanoMan VS microscope (Digital Instruments) in tapping mode.

Synthesis and Characterization of P1. To a 50 mL three-necked round-bottomed flask were added *N*,*N*′-bis(2-decyl-tetradecyl)-1,7-dibromo-3,4:9,10-perylene diimide (0.2 mmol, 245 mg), 2,6-diethynyldithieno[3,2-*b*:2′,3′-*d*]thiophene (0.2 mmol, 132 mg) and the mixture was deoxygenated with nitrogen for 30 min. $Pd(PPh_3)_4$ (20 μmol, 23 mg) and CuI (0.04 mmol, 7.6 mg) were added under nitrogen. Dry toluene (10 mL) and triethylamine (5 mL) were added by syringe and purged by nitrogen for 15 min. The dark red solution was stirred at 60 °C for 3 d under nitrogen atmosphere. The resulting dark green sticky solution was cooled down to room temperature. The mixture was extracted with CH_2Cl_2 (2 × 100 mL), washed with water (2 × 100 mL), and the extracts were dried over anhydrous $MgSO_4$. The solution was concentrated to 15 mL, then dropped into 200 mL of methanol. The dark green precipitate was filtered, and washed with methanol. Finally, the polymer was purified by size exclusion column chromatography over Bio-Rad Bio-Beads S-X1 eluting with THF. Polymer **P1** was dissolved in chloroform and filtered through a 0.22 μm Nylon-6 filter to remove the insoluble inpurities. After removal of the solvent to afford a dark green solid (219 mg, 84%). GPC: M_n = 15 000, M_w = 17 000, M_w/M_n = 1.1. ^{1}H NMR (300 MHz, $C_2D_4Cl_4$, 100 °C): δ 8.68 (br, 2H), 8.12 (br, 2H), 7.62 (br, 2H), 7.53 (br, 2H), 4.28 (br, 4H), 2.08 (br, 2H), 1.35 (br, 80H), 0.94 (br, 12H). Anal. Calcd for $(C_{86}H_{112}N_2O_4S_3)_n$: C, 77.43; H, 8.46; N, 2.10. Found: C, 76.62; H, 8.35; N, 1.92.

OFET Device Fabrication and Characterization. OFETs based on **P1** and **P2** films were fabricated in a top contact, bottom gate configuration. OFETs based on **P1** films were also fabricated in a bottom contact, bottom gate configuration.

Fabrication of Top Contact Bottom Gate Transistors. Heavily doped n-type Si wafers were used as substrates for the devices. SiO_2 layers of a capacitance of 11.5 nF/cm^2 as gate dielectrics were thermally grown on the Si substrates to a thickness of 300 nm. The substrates were cleaned sequentially with pure water, hot concentrated sulfuric acid-hydrogen peroxide solution (concentrated sulfuric acid/hydrogen peroxide water = 2:1), pure water, and isopropyl alcohol. Octadecyltrichlorosilane (OTS) was used as a self-assembled surface modifier for SiO_2. A 100 nm-thick (±10 nm) semiconductor film was spin-coated on top of the OTS-treated SiO_2 from 10 mg/mL chloroform solution of **P1** or **P2**. Then the as-spun thin film was annealed in vacuum oven at 170 °C for an hour. The channel length (L) and width (W) were 80 μm and 8.8 mm, respectively. Gold source and drain contacts (50 nm) were deposited on the organic layer through a shadow mask under high vacuum.

Fabrication of Bottom Contact Bottom Gate Transistors. Gold/Ti source and drain electrodes were patterned by photolithography and lift-off techniques on silicon/silica substrate. Before deposition of the semiconducting polymer, the substrate was modified using OTS monolayer. The polymer semiconductor layer was spin-coated from chloroform solution (10 mg/mL). The channel length (L) was 38 μm; and the channel width (W) was 1400 μm. Then the as-spun thin film was annealed in vacuum oven at 170 °C for an hour.

All OFETs were characterized with a Keithley 4200 semiconductor characterization system in air or in a N_2-filled glovebox. The mobility in the saturated regime was extracted from the following equation: $I_{DS} = C_i\mu(W/2L)(V_{GS} - V_T)^2$, where I_{DS} is the drain current, C_i is the capacitance per unit area of the gate dielectric layer, and V_{GS} and V_T are the gate voltage and threshold voltage, respectively.

ASSOCIATED CONTENT

Supporting Information

TGA and DSC curves of **P1**, μ_e /$\mu_{e,initial}$ vs time plot of **P1**-based top-contact bottom-gate devices, typical current−voltage characteristics for a bottom-contact bottom-gate device based on **P1**, typical current−voltage characteristics for a bottom-contact bottom-gate device based on **P2**, and μ_e vs time plot of bottom-contact bottom-gate devices based on **P1** and **P2**. This material is available free of charge via the Internet at http://pubs.acs.org.

AUTHOR INFORMATION

Corresponding Author

*E-mail: xwzhan@iccas.ac.cn (X.Z.); liuyq@iccas.ac.cn (Y.L.).

Notes

The authors declare no competing financial interest.

ACKNOWLEDGMENTS

This material is based upon work supported in part by the 973 Project (Grant 2013CB834702, 2011CB808401), NSFC (Grants 21025418, 50873107, 21021091), the Chinese Academy of Sciences, and Solvay S. A. The GIXRD data were obtained at 1W1A, Beijing Synchrotron Radiation Facility. The authors gratefully acknowledge the assistance of scientists of Diffuse X-ray Scattering Station during the experiments.

REFERENCES

(1) Cheng, Y.-J.; Yang, S.-H.; Hsu, C.-S. *Chem. Rev.* **2009**, *109*, 5868.
(2) Zaumseil, J.; Sirringhaus, H. *Chem. Rev.* **2007**, *107*, 1296.
(3) Tsao, H. N.; Müllen, K. *Chem. Soc. Rev.* **2010**, *39*, 2372.
(4) Beaujuge, P. M.; Fréchet, J. M. J. *J. Am. Chem. Soc.* **2011**, *133*, 20009.
(5) Bronstein, H.; Chen, Z.; Ashraf, R. S.; Zhang, W.; Du, J.; Durrant, J. R.; Shakya Tuladhar, P.; Song, K.; Watkins, S. E.; Geerts, Y.; Wienk, M. M.; Janssen, R. A. J.; Anthopoulos, T.; Sirringhaus, H.; Heeney, M.; McCulloch, I. *J. Am. Chem. Soc.* **2011**, *133*, 3272.
(6) Mei, J.; Kim, D. H.; Ayzner, A. L.; Toney, M. F.; Bao, Z. *J. Am. Chem. Soc.* **2011**, *133*, 20130.
(7) Tsao, H. N.; Cho, D. M.; Park, I.; Hansen, M. R.; Mavrinskiy, A.; Yoon, D. Y.; Graf, R.; Pisula, W.; Spiess, H. W.; Müllen, K. *J. Am. Chem. Soc.* **2011**, *133*, 2605.

(8) Chen, H.; Guo, Y.; Yu, G.; Zhao, Y.; Zhang, J.; Gao, D.; Liu, H.; Liu, Y. *Adv. Mater.* **2012**, *24*, 4618.
(9) Chen, Z.; Zheng, Y.; Yan, H.; Facchetti, A. *J. Am. Chem. Soc.* **2009**, *131*, 8.
(10) Briseno, A. L.; Mannsfeld, S. C. B.; Shamberger, P. J.; Ohuchi, F. S.; Bao, Z. N.; Jenekhe, S. A.; Xia, Y. N. *Chem. Mater.* **2008**, *20*, 4712.
(11) Yan, H.; Chen, Z.; Zheng, Y.; Newman, C.; Quinn, J. R.; Dotz, F.; Kastler, M.; Facchetti, A. *Nature* **2009**, *457*, 679.
(12) Zhang, L.; Di, C.-a.; Zhao, Y.; Guo, Y.; Sun, X.; Wen, Y.; Zhou, W.; Zhan, X.; Yu, G.; Liu, Y. *Adv. Mater.* **2010**, *22*, 3537.
(13) Guo, X.; Ortiz, R. P.; Zheng, Y.; Hu, Y.; Noh, Y.-Y.; Baeg, K.-J.; Facchetti, A.; Marks, T. J. *J. Am. Chem. Soc.* **2011**, *133*, 1405.
(14) Zhao, X.; Wen, Y.; Ren, L.; Ma, L.; Liu, Y.; Zhan, X. *J. Polym. Sci., Part A: Polym. Chem.* **2012**, *50*, 4266.
(15) Usta, H.; Facchetti, A.; Marks, T. J. *Acc. Chem. Res.* **2011**, *44*, 501.
(16) Anthony, J. E.; Facchetti, A.; Heeney, M.; Marder, S. R.; Zhan, X. *Adv. Mater.* **2010**, *22*, 3876.
(17) Zhao, X.; Zhan, X. *Chem. Soc. Rev.* **2011**, *40*, 3728.
(18) Zhan, X.; Facchetti, A.; Barlow, S.; Marks, T. J.; Ratner, M. A.; Wasielewski, M. R.; Marder, S. R. *Adv. Mater.* **2011**, *23*, 268.
(19) Huang, C.; Barlow, S.; Marder, S. R. *J. Org. Chem.* **2011**, *76*, 2386.
(20) Wurthner, F.; Stolte, M. *Chem. Commun.* **2011**, *47*, 5109.
(21) Zhan, X.; Tan, Z. A.; Domercq, B.; An, Z.; Zhang, X.; Barlow, S.; Li, Y.; Zhu, D.; Kippelen, B.; Marder, S. R. *J. Am. Chem. Soc.* **2007**, *129*, 7246.
(22) Zhan, X. W.; Tan, Z. A.; Zhou, E. J.; Li, Y. F.; Misra, R.; Grant, A.; Domercq, B.; Zhang, X. H.; An, Z. S.; Zhang, X.; Barlow, S.; Kippelen, B.; Marder, S. R. *J. Mater. Chem.* **2009**, *19*, 5794.
(23) Zhou, W. Y.; Wen, Y. G.; Ma, L. C.; Liu, Y. Q.; Zhan, X. W. *Macromolecules* **2012**, *45*, 4115.
(24) Guo, X.; Watson, M. D. *Org. Lett.* **2008**, *10*, 5333.
(25) Durban, M. M.; Kazarinoff, P. D.; Luscombe, C. K. *Macromolecules* **2010**, *43*, 6348.
(26) Huang, H.; Youn, J.; Ponce Ortiz, R.; Zheng, Y.; Facchetti, A.; Marks, T. *Chem. Mater.* **2011**, *23*, 2185.
(27) Durban, M. M.; Kazarinoff, P. D.; Segawa, Y.; Luscombe, C. K. *Macromolecules* **2011**, *44*, 4721.
(28) Silvestri, F.; Marrocchi, A. *Int. J. Mol. Sci.* **2010**, *11*, 1471.
(29) Dallos, T.; Beckmann, D.; Brunklaus, G.; Baumgarten, M. *J. Am. Chem. Soc.* **2011**, *133*, 13898.
(30) Yan, Q.; Zhao, D. *Org. Lett.* **2009**, *11*, 3426.
(31) Yue, W.; Zhen, Y.; Li, Y.; Jiang, W.; Lv, A.; Wang, Z. *Org. Lett.* **2010**, *12*, 3460.
(32) Kozma, E.; Munno, F.; Kotowski, D.; Bertini, F.; Luzzati, S.; Catellani, M. *Synth. Met.* **2010**, *160*, 996.
(33) Popere, B. C.; Della Pelle, A. M.; Thayumanavan, S. *Macromolecules* **2011**, *44*, 4767.
(34) Sajoto, T.; Tiwari, S. P.; Li, H.; Risko, C.; Barlow, S.; Zhang, Q.; Cho, J.-Y.; Brédas, J.-L.; Kippelen, B.; Marder, S. R. *Polymer* **2012**, *53*, 1072.
(35) Hahm, S. G.; Rho, Y.; Jung, J.; Kim, S. H.; Sajoto, T.; Kim, F. S.; Barlow, S.; Park, C. E.; Jenekhe, S. A.; Marder, S. R.; Ree, M. *Adv. Funct. Mater.* **2012**, DOI: 10.1002/adfm.201202065.
(36) Wurthner, F.; Stepanenko, V.; Chen, Z.; Saha-Moller, C. R.; Kocher, N.; Stalke, D. *J. Org. Chem.* **2004**, *69*, 7933.
(37) Becke, A. D. *J. Chem. Phys.* **1993**, *98*, 5648.
(38) Lee, C.; Yang, W.; Parr, R. G. *Phys. Rev. B* **1988**, *37*, 785.
(39) *Gaussian 09, Revision A.1* Frisch, M. J.; Trucks, G. W.; Schlegel, H. B.; Scuseria, G. E.; Robb, M. A.; Cheeseman, J. R.; Scalmani, G.; Barone, V.; Mennucci, B.; Petersson, G. A.; Nakatsuji, H.; Caricato, M.; Li, X.; Hratchian, H. P.; Izmaylov, A. F.; Bloino, J.; Zheng, G.; Sonnenberg, J. L.; Hada, M.; Ehara, M.; Toyota, K.; Fukuda, R.; Hasegawa, J.; Ishida, M.; Nakajima, T.; Honda, Y.; Kitao, H.; Nakai, O.; Vreven, T.; Montgomery, J. A., Jr.; Peralta, J. E.; Ogliaro, F.; Bearpark, M.; Heyd, J. J.; Brothers, E.; Kudin, K. N.; Staroverov, V. N.; Kobayashi, R.; Normand, J.; Raghavachari, K.; Rendell, A.; Burant, J. C.; Iyengar, S. S.; Tomasi, J.; Cossi, M.; Rega, N.; Millam, J. M.; Klene, M.; Knox, J. E.; Cross, J. B.; Bakken, V.; Adamo, C.; Jaramillo, J.; Gomperts, R.; Stratmann, R. E.; Yazyev, O.; Austin, A. J.; Cammi, R.; Pomelli, C.; Ochterski, J. W.; Martin, R. L.; Morokuma, K.; Zakrzewski, V. G.; Voth, G. A.; Salvador, P.; Dannenberg, J. J.; Dapprich, S.; Daniels, A. D.; Farkas, ö.; Foresman, J. B.; Ortiz, V. J.; Cioslowski, J.; Fox, D. J. Gaussian, Inc.: Wallingford, CT, 2009.
(40) Tan, Z. A.; Zhou, E.; Zhan, X.; Wang, X.; Li, Y.; Barlow, S.; Marder, S. R. *Appl. Phys. Lett.* **2008**, *93*, 073309.
(41) Zhou, E.; Tajima, K.; Yang, C. H.; Hashimoto, K. *J. Mater. Chem.* **2010**, *20*, 2362.
(42) Kozma, E.; Kotowski, D.; Bertini, F.; Luzzati, S.; Catellani, M. *Polymer* **2010**, *51*, 2264.
(43) Facchetti, A. *Chem. Mater.* **2011**, *23*, 733.
(44) Lei, T.; Cao, Y.; Fan, Y.; Liu, C.; Yuan, S.; Pei, J. *J. Am. Chem. Soc.* **2011**, *133*, 6099.
(45) Huang, X.; Zhu, C.; Zhang, S.; Li, W.; Guo, Y.; Zhan, X.; Liu, Y.; Bo, Z. *Macromolecules* **2008**, *41*, 6895.